ELSEVIER

Journal of Nuclear Materials 276 (2000) 166–177

journal of nuclear materials

www.elsevier.nl/locate/jnucmat

Interaction and accumulation of glissile defect clusters near dislocations

N.M. Ghoniem[a,*], B.N. Singh[b], L.Z. Sun[a], T. Díaz de la Rubia[c]

[a] *Mechanical and Aerospace Engineering Department, University of California at Los Angeles, Los Angeles, CA 90095-1597, USA*
[b] *Risø National Laboratory, DK-4000, Roskilde, Denmark*
[c] *Lawrence Livermore National Laboratory, Livermore, CA 94550, USA*

Abstract

Accumulation of nano-size prismatic defect clusters near slip-dislocations results from their mutual elastic interaction. We present here 3-D isotropic elasticity calculations for the interaction energy between radiation-induced nano-size prismatic loops and grown-in dislocation loops. The current treatment extends the work of Trinkaus et al. in two respects. First, a computational method for full 3-D analysis of interaction energies in bcc Fe and fcc Cu is developed. Second, the theoretical method of Kroupa is computationally implemented for rigorous calculations of force, torque and induced surface energy on defect clusters. It is shown that small clusters are trapped within a zone of ~10 nm in bcc Fe, and ~20 nm in fcc Cu at room temperature, in rough agreement with experimental observations. Clusters can be absorbed in the core of grown-in dislocations because of unbalanced moments, which provide sufficient energy for rotation of their Burgers vectors in a zone of 2–3 nm in Fe. Near the dislocation core (within a few nanometers), sessile defect clusters in Cu are shown to convert to a glissile configuration.

1. Introduction

The phenomenon of radiation hardening has been an interesting subject of both experimental and theoretical investigations for more than 40 years. It is well documented that, when metals and alloys are irradiated at temperatures below the recovery stage V (i.e., $<0.3\ T_m$, where T_m is the melting temperature), their upper yield stresses increase significantly whereas their ductility decrease drastically. A common feature of the stress–strain curves obtained during tensile tests of irradiated metals and alloys is the occurrence of a yield drop, immediately after the upper yield stress. The occurrence of the yield drop is dependent on the irradiation dose, material and irradiation temperature (see [1] for a review). In most polycrystalline metals and alloys, the yield drop is followed by plastic instability with negative work hardening. This suggests that the plastic deformation in these irradiated materials is initiated in a localized and inhomogeneous fashion. The fact that the plastic deformation occurs in a localized and inhomogeneous fashion has been confirmed by post-deformation microstructure investigations, showing that the deformation is concentrated in inhomogeneously distributed narrow bands, commonly known as 'cleared' channels (see, e.g., [2–4]). These investigations also showed that there is no evidence of dislocation generation during deformation in the regions between the cleared channels.

Under neutron or charged particle irradiation, nano-size point defect clusters nucleate directly from atomic collision cascades in irradiated materials. Once these clusters nucleate, they take the shape of small prismatic dislocation loops of radial dimensions in the range of 1–3 nm (i.e., containing several to ~100 atoms). Molecular dynamics (MD) computer simulations [5–9] suggest that, in both bcc and fcc metals, these clusters of self-interstitial atoms (SIAs) can be rather mobile, and that they migrate predominantly along close-packed crystallographic directions. The most stable clusters in bcc Fe are glissile sets of co-linear $\langle 1\,1\,1\rangle$-crowdions, with a dislocation loop character of $(a/2)\langle 1\,1\,1\rangle\{1\,1\,1\}$ [5]. In fcc Cu, hexagonal faulted Frank loops of type $(a/3)\langle 1\,1\,1\rangle\{1\,1\,1\}$

* Corresponding author. Tel.: +1-310 825 4866; fax: +1-310 206 4830.
E-mail address: ghoniem@ucla.edu (N.M. Ghoniem)

0022-3115/00/$ - see front matter
PII: S0022-3115(99)00176-2

[5], as well as perfect loops [8] are found to be stable and sessile. Vacancy clusters in Cu are shown as {1 1 1}-platelets of stacking fault tetrahedra (SFTs) [5]. Experimental evidence [1,10] suggest that, under electron irradiation, with defect clusters not directly produced in collision cascades, grown-in dislocations are not heavily decorated with small defect clusters. The work of Sigle et al. [10] indicates that only SFTs are found within 20 nm of dislocation cores, and their position is on the compression side of edge dislocations.

In view of these experimental findings on post-irradiation deformation behavior and post-deformation microstructure, the problem of radiation hardening has been recently re-analyzed and treated in terms of cascade induced source hardening (CISH) model [1]. The main thesis of the CISH model is that, during irradiation, most of the Frank–Read (FR) sources (i.e., grown-in dislocations) are locked by an 'atmosphere' of small interstitial loops produced in collision cascades. The initiation of plastic deformation and the upper yield stress is then related to the stress that is necessary to unlock these decorated dislocations in order to operate as FR sources. To evaluate the model, a simple estimate was made of the 'stand-off' or 'absorption' distance (from the lead dislocation) at which the decoration may start [1]. Assuming an un-dissociated edge dislocation to be the lead dislocation, a lower-bound value of this distance was found to be of the order of the radius of the loops forming the decoration. At distances smaller than the stand-off distance, the small loops may change their Burgers vector and get absorbed in the edge dislocation core.

Trinkaus et al. have examined the central question of the formation of dislocation decoration [11,12]. They provided analytical estimates for elastic interactions between point defects and small defect clusters with an infinitely long, straight edge dislocation. In addition, the accumulation of glissile loops near the edge dislocation and the conditions for their absorption was estimated. Results of these calculations were used to determine the critical unlocking stress of an edge dislocation from a row of loops, as well as a loop ensemble approximated by dislocation dipoles.

Fig. 1 shows a TEM micrograph of pure single crystal Mo irradiated with fission neutrons at 320 K [11,13], illustrating formation of dislocation loop 'rafts' already at a dose level of ~0.16 dpa. Grown-in (slip) dislocations are clearly decorated with small defect clusters, without any preference to either side of pre-existing dislocations. From crude TEM micrograph observations, the attraction (decoration) zone appears to be on the order of 10 nm in bcc metals [13], and about 20 nm in fcc metals [10]. While defect clusters nucleate homogeneously under electron irradiation, they can be directly produced heterogeneously by collision cascades under ion or neutron irradiation. Experimental evidence

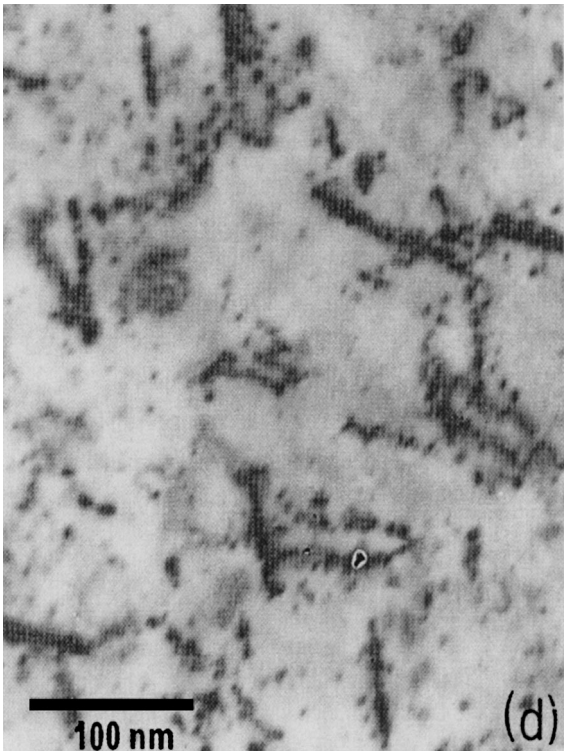

Fig. 1. A TEM micrograph of pure single crystal Mo irradiated with fission neutrons at 320 K (after Refs. [1,13]) to a displacement dose level of 0.16 dpa.

of their interaction with dislocations is consistent with a high degree of cluster mobility. Thus, decoration of existing dislocations with nano-size defect clusters and the formation of rafts of small dislocation loops (Fig. 1) is a consequence of in-cascade nucleation, followed by coherent transport along closely packed crystallographic directions.

It is well established that neutron irradiation leads to a substantial increase in the yield strength and hardening of metals. This phenomenon is particularly severe at low temperatures (i.e., below recovery stage V). The decoration of slip dislocations with defect clusters appears to be the controlling mechanism for blocking dislocation generation on its glide plane. Moreover, once plastic deformation commences, it is observed to be rather heterogeneous and concentrated in 'soft' deformation channels, while the vast majority of the matrix is in a state of elastic deformation. The onset of this type of plastic instability is thus associated with the initiation and propagation of cleared channels that are nearly free of defect clusters. Decoration of dislocations with irradiation-produced defect clusters is possibly the root cause of localized plastic deformation, leading to premature fracture. This qualitative picture can explain the initial radiation hardening and the

subsequent onset of flow localization. However, quantitative determination of the detailed mechanisms by which the phenomenon occurs remains largely unexplored.

Recently, a new computational method has been developed [14,15] for accurate evaluation of the elastic field of dislocation aggregates in complex 3-D geometry. The method extends the capabilities of 2-D estimates of elastic field variables in realistic material geometry, and enables calculations of displacements, strain, stress, interaction and self-energies, and finally, the work associated with rotation and translation of defect clusters. In this paper, we apply the numerical method developed by Ghoniem [14] and Ghoniem and Sun [15] to examine the mechanisms of interaction between small defect clusters and slip dislocation loops. In this connection, the approach we present here is a further development of the foundational work of Trinkaus et al. [11,12]. The additional features of the present investigation are summarized as:

1. Calculation of all elastic field variables in three dimensions, thus enabling determination of complex interaction possibilities between defect clusters and dislocations.
2. Incorporation of the elastic interaction energy into the energy balance on dissociated dislocation clusters in fcc metals. In this fashion, we are able to address the probability of prismatic loop unfaulting in irradiated Cu.
3. Numerical evaluation of the mechanical work necessary to rotate small defect clusters. Thus, they can align themselves in directions favorable for absorption into dislocation cores. This method can accurately determine the 'absorption' zone.
4. Accurate determination of the self and interaction energies between multiple cluster/ dislocation configurations. This capability allows determination of the conditions for 'loop raft' formation in some bcc metals.

In the following, we present the salient features of the new computational method for determination of dislocation/cluster geometry and elastic interaction fields. Results of interaction energy surfaces and iso-energy contours will then be shown in Sections 3 and 4 for bcc Fe and fcc Cu, respectively. The contours that delineate the regions of attraction around dislocation loops (i.e., 'trapping zones'), as well as the regions of cluster absorption (i.e. 'absorption zones') will also be given in the same section. We also present the results of our calculations for the temperature dependence of the attraction zone around several pure metal. Furthermore, we discuss the possibility of sessile dislocation cluster unfaulting in the stress field of grown-in dislocations in fcc Cu. Finally, conclusions and discussion of outstanding issues are presented in Section 5.

2. Dislocation geometry and elastic field

2.1. Differential geometry of dislocations and clusters

The geometry of arbitrary shape dislocation loops is described as a sequence of segments, continuous to second parametric derivative (C^2 continuity). A single curved dislocation segment is shown in Fig. 2, for the sake of defining 3-D coordinates and notation used throughout. Details of the method are given in Ref. [15]. Calculations of all elastic field variables depend on the radius vector **R** between a source point on the loop at $\hat{\mathbf{x}}$, and a field point in the crystal at point **x**. To bring about the main physical features of the elastic interaction problem, without undue geometric complexities, we perform calculations for simplified yet typical configurations. In Fig. 3, a typical geometric representation for interaction between prismatic defect clusters and deformation slip loops on the primary glide plane of bcc crystals is shown. The medium is assumed to be infinite and elastically isotropic, but the cube size of Fig. 3 is taken as $1000a$, where a is the lattice parameter. The slip loop is at the center of the cube, and has a diameter of $400a$, while the defect clusters are assumed to have a diameter of 3 nm. The slip loop in fcc crystals is assumed to be on the $\langle 111\rangle$-plane, with Burgers vector $(a/2)\langle 110\rangle$ as schematically illustrated in Fig. 4. The habit plane of defect clusters in fcc crystals is (110), while their Burgers vector is of the $(a/2)\langle 110\rangle$-type. Several combinations of loop and cluster Burgers vectors have been studied to determine the geometric symmetry of interaction energy iso-surfaces in both fcc and bcc crystals.

A dislocation loop of arbitrary 3-D shape is discretized into parametric segments. For each segment (j), we choose a set of generalized coordinates $q_{ik}^{(j)}$ and the corresponding shape functions $N_i(u)$ to represent the configuration of the segment, i.e.,

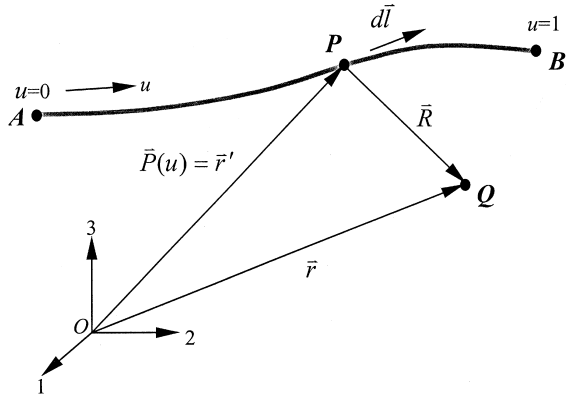

Fig. 2. Coordinate system and notation for geometric representation of dislocation loops.

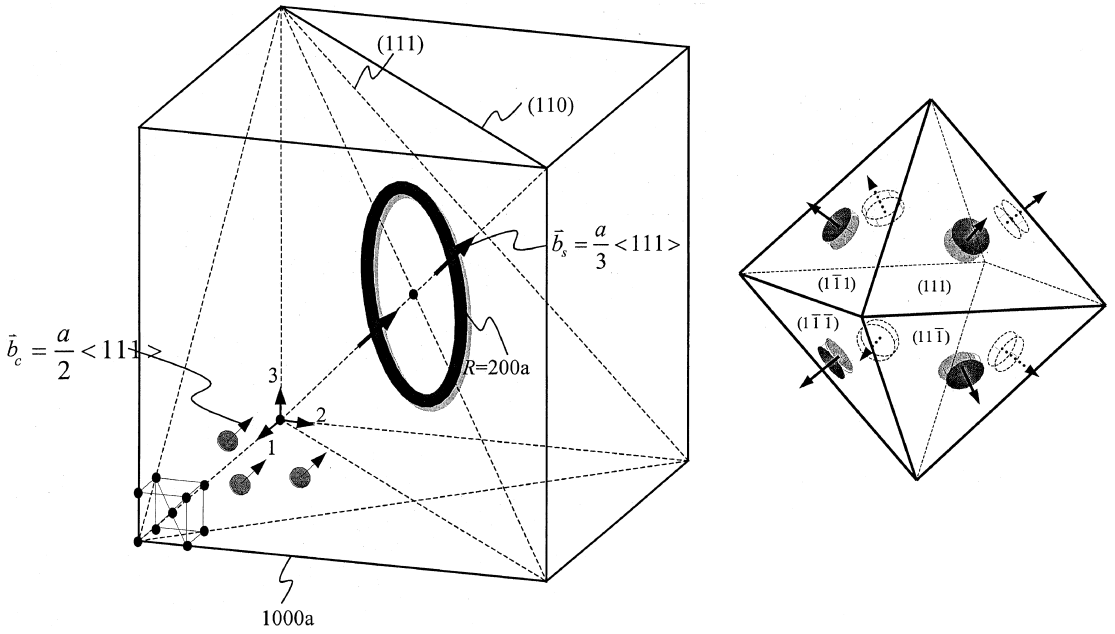

Fig. 3. Geometry of a prototypical slip loop and interacting defect clusters in bcc crystals.

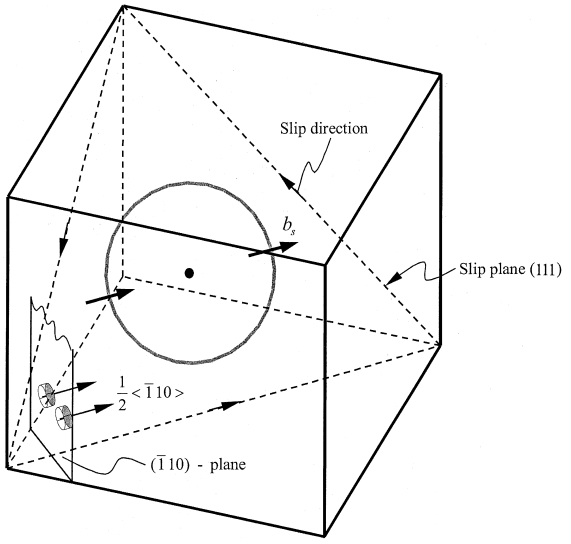

Fig. 4. Geometry of a prototypical slip loop and interacting defect clusters in fcc crystals.

$$\hat{x}_k^{(j)}(u) = N_i(u) q_{ik}^{(j)} \qquad \text{(sum over } (i) \text{ is implied)}, \tag{1}$$

where $\hat{x}_k^{(j)}(u)$ is the Cartesian position of a point on segment (j), in the kth-direction ($k=1$, 2, 3), and $0 \leqslant u \leqslant 1$ is a suitable parameter. Specific Degrees of Freedom (DOF) are denoted by $(i = 1, 2, \ldots, I)$. One convenient way of parametrizing the segment is to use cubic splines as shape functions $N_i(u)$, with $I=4$. They take the form:

$$\begin{aligned} N_1(u) &= 2u^3 - 3u^2 + 1, \\ N_2(u) &= -2u^3 + 3u^2, \\ N_3(u) &= u^3 - 2u^2 + u, \\ N_4(u) &= u^3 - u^2. \end{aligned} \tag{2}$$

More general parametric forms are discussed in Ref. [15]. In the present parametric case, the generalized coordinates $q_{ik}^{(j)}$ are just the position and tangent vectors, associated with the beginning B and end E nodes on segment (j).

2.2. Elastic field and interaction energies

Following Kröner [16] and DeWit [17], the elastic field tensors (strain ε_{ij} and stress σ_{ij}) of a dislocation loop are given by line integrals over the dislocation loop line vector. We extend their general theory to the specific case of parametric dislocation loop representation. The strain components are

$$\varepsilon_{ij} = \frac{1}{8\pi} \oint_C \Big\{ -\frac{1}{2} \big(\in_{jkl} b_i R_{,l} + \in_{ikl} b_j R_{,l} - \in_{ikl} b_l R_{,j} - \in_{jkl} b_l R_{,i} \big)_{,pp} + \frac{1}{1-\nu} \in_{kmn} b_n R_{,mij} \Big\} \mathrm{d}l_k, \tag{3}$$

where $R = \|\mathbf{R}\| = \|x - \hat{x}\|$.

Since the linear stress–strain relationship is $\sigma_{ij} = 2G\varepsilon_{ij} + \lambda\varepsilon_{rr}\delta_{ij}$, the stress tensor is also obtained as a line integral, of the general form [16,17]

$$\sigma_{ij} = \frac{Gb_n}{4\pi}\oint_C \left[\frac{1}{2}R_{,mpp}\left(\in_{jmn} \mathrm{d}l_{i'} + \in_{imn} \mathrm{d}l_{j'}\right) + \frac{m}{m-1}\in_{kmn}\left(R_{,ijm} - \delta_{ij}R_{,ppm}\right)\mathrm{d}l_{k'}\right], \tag{4}$$

where G is the shear modulus, b_n the components of Burgers vector, $R_{,ijk}$ are derivatives of the radius vector norm between a loop point at $\hat{\mathbf{x}}$ and a filed point $\mathbf{x}$, $\mathrm{d}l_{i'}$ are differential line elements along the dislocation line vector, and $\in_{ijk}$ is the permutation tensor. Ghoniem [14] developed explicit forms for the integrals of general parametric dislocation loops. An efficient numerical integration scheme has also been developed for calculations of the stress field, as a fast summation by Ghoniem and Sun [15]. Their results read

$$\sigma_{ij} = \frac{G}{4\pi}\sum_{\gamma=1}^{N_{\mathrm{loop}}}\sum_{\beta=1}^{N_s}\sum_{\alpha=1}^{Q_{\max}} b_n w_\alpha \left\{\frac{1}{2}R_{,mpp}\left(\in_{jmn}\hat{x}_{i,u} + \in_{imn}\hat{x}_{j,u}\right) + \frac{1}{1-v}\in_{kmn}\left(R_{,ijm} - \delta_{ij}R_{,ppm}\right)\hat{x}_{k,u}\right\}, \tag{5}$$

where N_{loop}, N_s, and $Q_{\max}$ are the total number of loops, segments, and Guassian quadrature, respectively. w_α is the quadrature weight, and $\hat{x}_{j,u}$ are parametric derivatives of the Cartesian components of the vector $\hat{\mathbf{x}}$, which describes the loop geometry.

The interaction energy of two dislocation loops over the volume V of the material is defined as

$$E_I = \int_V \sigma_{ij}^{(1)}\varepsilon_{ij}^{(2)}\,\mathrm{d}V \tag{6}$$

in which $\sigma_{ij}^{(1)}$ is the stress arising from the first dislocation and $\varepsilon_{ij}^{(2)}$ the strain originating in the other. For the present study, if the second loop (defect cluster) is assumed to be infinitesimal, the interaction energy can be simplified to [18]

$$E_i = \delta A^{(2)} n_i^{(2)} \sigma_{ij}^{(1)} b_j^{(2)}, \tag{7}$$

where $n_i^{(2)}$ is the unit normal vector to the defect cluster habit plane of area $\delta A^{(2)}$. By substituting Eq. (5) into Eq. (7) with $N_{\mathrm{loop}} = 1$, we can finally compute the interaction energy of the cluster, designated with the superscript (2), and the slip loop, of Burgers vector $b_n^{(1)}$, as

$$E_I = \frac{G\delta A^{(2)} n_i^{(2)} b_j^{(2)}}{4\pi}\sum_{\beta=1}^{N_s}\sum_{\alpha=1}^{Q_{\max}} b_n^{(1)} w_\alpha \left\{\frac{1}{2}R_{,mpp}\left(\in_{jmn}\hat{x}_{i,u} + \in_{imn}\hat{x}_{j,u}\right) + \frac{1}{1-v}\in_{kmn}\left(R_{,ijm} - \delta_{ij}R_{,ppm}\right)\hat{x}_{k,u}\right\}. \tag{8}$$

In the above equation, we assume that the stress tensor of the grown-in (slip) dislocation loop is constant over the cross-section of a small point-defect cluster. In case we treat one single vacancy or interstitial atom as a center of dilatation, the interaction energy simplifies to [19]

$$E_I = -\frac{4}{9}\pi r_0^3 \varepsilon_{ii}^{(2)} \sigma_{jj}^{(1)}, \tag{9}$$

where $\varepsilon_{ii}^{(2)}$ is the dilatation and r_0 is the effective radius of a point defect. The above equation does not reveal dependence of the interaction energy surface on the orientation of the cluster Burgers vector, unlike Eq. (8).

2.3. Force, torque and induced surface tension on defect clusters

The total force F and its torque M on the cluster due to the slip loop can be expressed in component form as [18]

$$F_i = -n_j^{(2)}\sigma_{jk,i}^{(1)} b_k^{(2)} \delta A^{(2)}, \tag{10}$$

$$M_i = -\in_{ijk} n_j^{(2)} b_l^{(2)} \sigma_{lk}^{(1)} \delta A^{(2)}. \tag{11}$$

Extending the infinitesimal loop approximation of Kroupa [18], where we introduce geometric parametrization of the loops and the fast sum formulation, we obtain the following computational forms for the Cartesian components (i) of the total force and torque on the defect cluster:

$$F_i = -\frac{G\delta A^{(2)} n_j^{(2)} b_k^{(2)}}{4\pi}\sum_{\beta=1}^{N_s}\sum_{\alpha=1}^{Q_{\max}} b_n^{(1)} w_\alpha \times \left\{\frac{1}{2}R_{,mpp}\left(\in_{kmn}\hat{x}_{j,u} + \in_{jmn}\hat{x}_{k,u}\right) + \frac{1}{1-v}\in_{lmn}\left(R_{,jkm} - \delta_{jk}R_{,ppm}\right)\hat{x}_{l,u}\right\}_{,i}, \tag{12}$$

$$M_i = -\frac{\in_{ijk} G\delta A^{(2)} n_j^{(2)} b_l^{(2)}}{4\pi}\sum_{\beta=1}^{N_s}\sum_{\alpha=1}^{Q_{\max}} b_n^{(1)} w_\alpha \times \left\{\frac{1}{2}R_{,mpp}\left(\in_{kmn}\hat{x}_{l,u} + \in_{lmn}\hat{x}_{k,u}\right) + \frac{1}{1-v}\in_{qmn}\left(R_{,lkm} - \delta_{lk}R_{,ppm}\right)\hat{x}_{q,u}\right\}. \tag{13}$$

As the defect cluster moves closer to the core of the slip loop, the turning moment (torque) on its habit plane increases, as given by Eq. (13). If the amount of mechanical work of rotation exceeds a critical value (taken as 0.1 eV/crowdion, as estimated by MD calculations of Forman [20]), it is assumed to change its Burgers vector and habit plane and move to be incorporated into the dislocation core. The mechanical work for cluster

rotation is equated to this critical value, (i.e., $\delta W = \int_{\theta_1}^{\theta_2} M_i \, d\theta_i = \Delta U_{crit}$). The critical surface for cluster rotation and hence subsequent absorption into the dislocation core may thus be determined.

The large local stress field close to the core of a dislocation loop can result in an induced surface tension on the loop [18]. This additional (or induced) surface tension is given by the amount of work done in expanding the surface area of the loop in the existing filed: $\gamma' = n_i^{(2)} \sigma_{ij}^{(1)} b_j^{(2)}$. Since the stress field and cluster orientation are both involved in determining the induced surface tension, the energy value can be either positive or negative. Thus, the critical unfaulting radius for a typical dislocation cluster may increase or decrease from its unstressed value, depending on whether the additional virtual work adds or subtracts from the stacking fault energy. For a circular Frank loop to unfault, the loop containing the fault and its perfect counterpart is attained by an additional Schokley partial dislocation of type: $(a/6)\langle 1\,1\,\bar{2}\rangle$. The required energy difference for loop unfaulting is given by

$$\Delta E = \pi r^2 \gamma + n_i^{(2)} \sigma_{ij}^{(1)} b_j^{(2)} - \frac{rGa^2}{24}\left(\frac{2-v}{1-v}\right)\ln\left(\frac{2r}{\varepsilon_0}\right), \tag{14}$$

where ε_0 is a dislocation core radius (taken as half of the Burgers vector), and a is the lattice parameter.

3. Results for bcc crystals

Fig. 5(a) shows contours of the interaction energy between interstitial defect clusters of Burgers vector $(a/2)\langle 1\,\bar{1}\,1\rangle$ and a proto-typical slip loop on the $\langle 1\,1\,0\rangle$-plane in bcc-Fe at room temperature. The plane of the contours is defined by the vectors $\langle 0\,0\,1\rangle$ and $\langle 1\,\bar{1}\,0\rangle$, and the energy units are all given in (kT/cluster atom). In this particular orientation of the cluster's Burgers vector, the iso-energy contours have radial symmetry with respect to the center of the $[1\,\bar{1}\,0]$-plane, as can be seen from Fig. 5(b). The symmetry properties of the iso-energy surfaces depend on the relative orientations of the slip loop and cluster Burgers vectors.

Clusters are shown to glide along close packed-directions with very low activation energy [5,8]. It is argued in Ref. [8] that motion of an entire cluster is unlikely to be described as a diffusion process. In Ref. [11,12], cluster motion has been modeled as a diffusion process in the drift field of grown-in dislocations. In this fashion, the 'trapping zone' of a cluster close to a dislocation has been determined when the cluster interaction energy is greater than (kT). In the present estimate, we assume the crowdions within the cluster vibrate with an average thermal energy of (kT). They can migrate randomly along close package directions as dynamic crowdions, with some coherence amongst them. Therefore, we plot the interaction energy contours in units of (kT) per crowdion in the cluster. If the magnitude of the interaction energy per atom is higher than (kT) and is attractive (i.e., negative), the cluster cannot escape from within the attractive zone by random walk. It will oscillate within this surface, until it loses its energy and gets trapped indefinitely. This scenario of cluster motion in the stress field of dislocations my be too simplistic, and requires further atomistic investigations by the MD and MC methods. Since there are three other symmetries for the energy surfaces around the dislocation loop, the exact shape of the trapping zone will be a complicated superposition of the four configurations. Constant

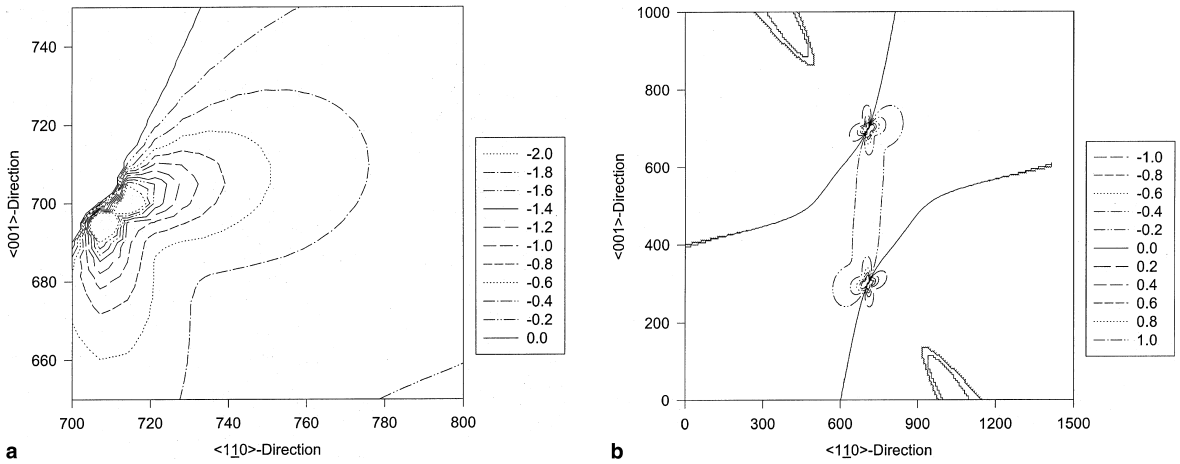

Fig. 5. (a) Local iso-energy contours for the interaction energy between $(a/2)\langle 1\,\bar{1}\,1\rangle$-type clusters and the bcc slip loop. Energy levels are in units of (kT/atom), (b) global iso-energy contours for the interaction energy between $(a/2)\langle 1\,\bar{1}\,1\rangle$-type clusters and the bcc slip loop. Energy levels are in units of (kT/ atom).

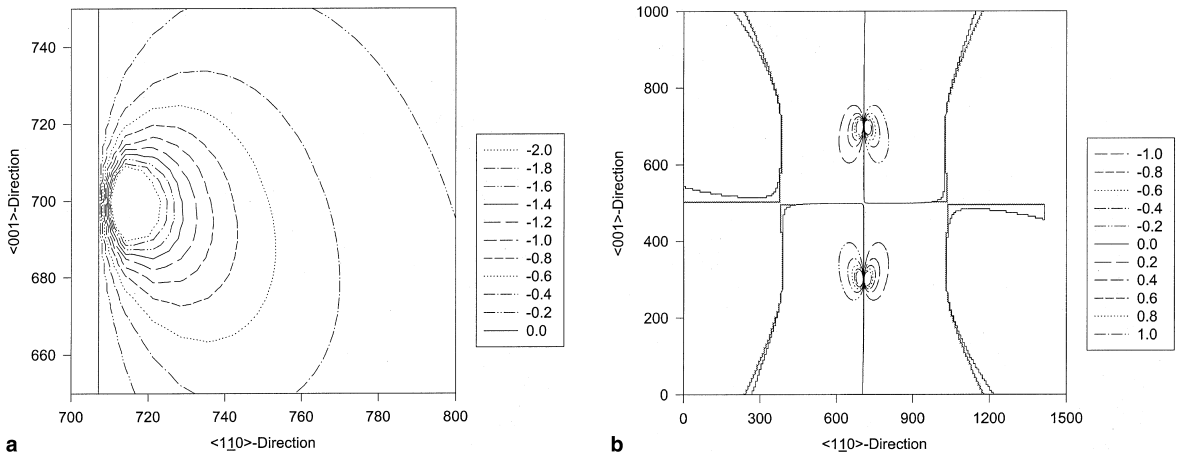

Fig. 6. Global iso-energy contours for the interaction energy between $(a/2)\langle 1\,1\,1\rangle$-type clusters and the bcc slip loop. Energy levels are in units of (kT/atom).

energy contours for cluster orientations: $\langle 1\,1\,1\rangle$, $\langle \bar{1}\,\bar{1}\,1\rangle$ and $\langle \bar{1}\,1\,1\rangle$ are shown in Figs. 6–8, respectively. Since the cluster habit plane vector $n_i^{(2)}$ is always along the same direction as its Burgers vector $b_i^{(2)}$ because it is prismatic, and the energy is a quadratic function of their product (see Eq. (8)), then the four other remaining cluster orientations of Fig. 3 will be redundant.

The 3-D surface bounding a value of $-$kT/atom is considered a trapping surface, and clusters which enter into this zone will oscillate within it. A 3-D picture of one of the four trapping zones in bcc at room temperature is shown in Figs. 9 and 10 for high and low interaction energy magnitudes, respectively. It is clear that the zone assumes a crescent-shape, of maximum width

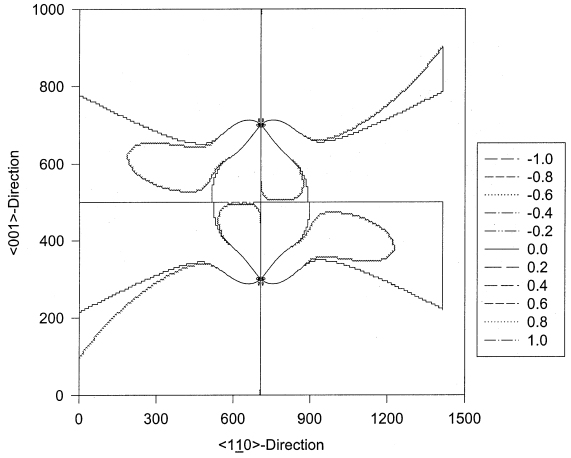

Fig. 8. Global iso-energy contours for the interaction energy between $(a/2)\langle \bar{1}\,1\,1\rangle$-type clusters and the bcc slip loop. Energy levels are in units of (kT/atom).

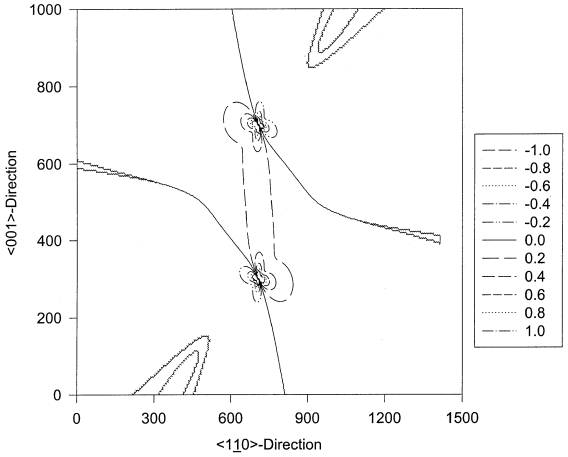

Fig. 7. Global iso-energy contours for the interaction energy between $(a/2)\langle \bar{1}\,\bar{1}\,1\rangle$-type clusters and the bcc slip loop. Energy levels are in units of (kT/atom).

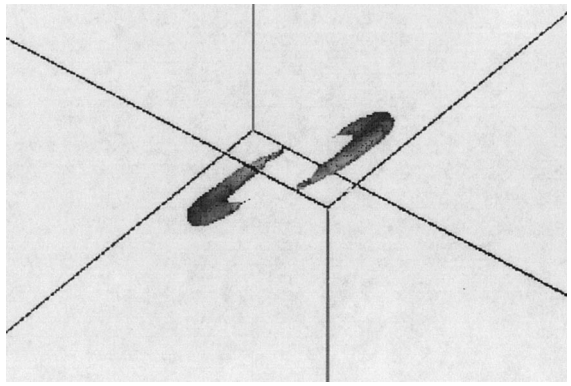

Fig. 9. 3-D iso-energy surface for bcc Fe. The value of the constant energy for this surface is -0.2 kT. It shows the shape of the trapping zones above and below the slip plane.

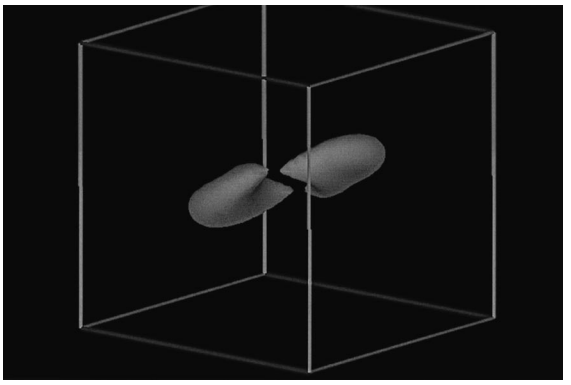

Fig. 10. 3-D iso-energy surface for bcc Fe. The value of the constant energy for this surface is -0.01 kT.

around the edge component of the slip loop. The trapping zone size diminishes for mixed character segments on the slip loop, and vanishes at the purely screw component. Generally, the surface bounding a value of -kT is considered a trapping surface, and clusters that enter into this zone will oscillate within the crystal volume bound by this surface.

It is found that this stand-off zone is about one cluster diameter $\sim$3 nm. Figs. 9 and 10 indicate that the maximum capture zone size (at the edge component) decreases with temperature, and is greater for fcc-Cu as compared to bcc-Fe. Both observations result from an increase in the cluster thermal energy, and a decrease in its modulus with temperature.

As a result of the non-uniform force distribution on crowdions composing the core of the dislocation cluster, it will experience a net torque, as computed by Eq. (13) above. The habit plane of the cluster will thus tend to rotate so as to minimize the total system energy. However, cluster rotation is associated with stretching of the interatomic distances, and will thus require a critical amount of energy to overcome this configurational barrier. Forman [20] estimated that the critical energy for this process is on the order of 0.1-eV/crowdion in Fe. We calculate the 3-D moments on approaching clusters via Eq. (13), and then assume that it will undergo rotation to change the direction of its Burgers vector. The amount of this virtual work done by the cluster is compared to the critical value computed by Forman [20]. If this amount of work exceeds the critical value, the cluster is assumed to make a final change in its Burgers vector, and head towards the dislocation core. It is further assumed here that the cluster may have to undergo another rotation to align its Burgers vector, subsequent re-arrangement of the cluster habit plane resulting in absorption is certain to happen, because the interaction energy for attraction and rotation will dramatically increase after the first flip. Figs. 11(a) and (b) show iso-work contours for clusters in bcc Fe. On each point on the contour, the dislocation will perform the same amount of work on the cluster to rotate its Burgers vector towards its core. The critical surface for Burgers vector rotation is seen to have an extent of only 2–3 nm from the dislocation core.

4. Results for fcc crystals

The slip plane in the case of fcc Cu is the $\{1\,1\,1\}$-family, and the slip direction is $\langle 1\,1\,0\rangle$. Thus, glissile prismatic defect clusters in Cu of the $(a/2)\langle \bar{1}\,1\,0\rangle$-type

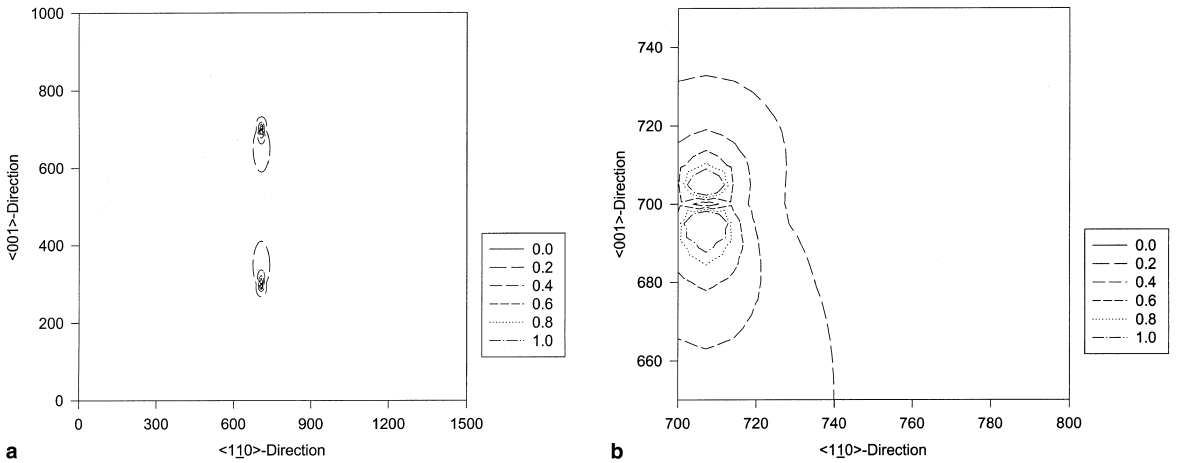

Fig. 11. (a) Global iso-work contours for bcc Fe. On each point on the contour, the dislocation will perform the same amount of work on the cluster to rotate its Burgers vector towards its core; (b) local iso-work contours for the same conditions as in (a). Contour values are in units of 0.1 eV/ atom. The critical surface for Burgers vector rotation is thus the zone enclosed by the contour at a value of unity.

have been investigated by Osetsky et al., using MD [8]. However, for these clusters to be glissile, they must first unfault and change their Burgers vector from the $\langle 1\,1\,1\rangle$ sessile direction to the $(a/2)\langle\bar{1}\,1\,0\rangle$-direction on the slip plane. We will show later that this may be possible if clusters grow to a large enough size in the presence of an external stress field. Fig. 12 shows iso-interaction energy contours between defect clusters and the slip loop in fcc Cu. The size of the trapping zone in this case is about twice that of the Fe case, mainly due to differences in their elastic module and lattice constants. It is also observed that the iso-energy contours are not symmetric with respect to the dislocation core, as is the case for the straight dislocation calculations of Trinkaus et al. [10,11]. This is mainly due to the influence of the loop curvature (self-energy) on the magnitude of the interaction energy. The higher the curvature, the larger the degree of asymmetry. Fig. 13 shows contours of iso-work for rotation of the cluster's Burgers vector, and their eventual absorption in fcc Cu. The size of the critical zone is seen to be about 20 lattice parameters. To gain a more visual appreciation of where clusters would be trapped with respect to a slip loop on the $[1\,1\,1]$-plane, Fig. 14 shows a 3-D iso-energy surface for Cu. The

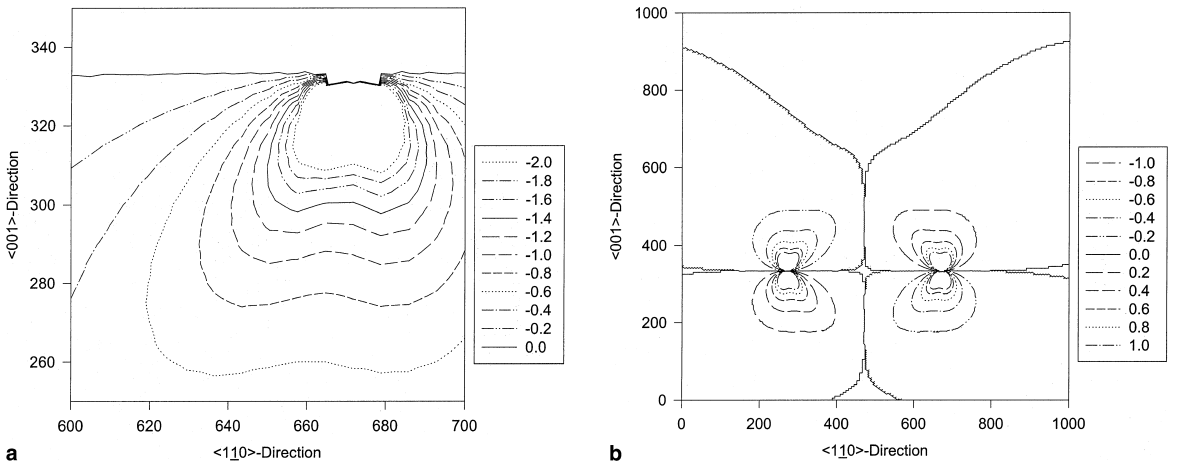

Fig. 12. (a) Local iso-energy contours for the interaction energy between $(a/2)\langle\bar{1}\,1\,1\rangle$-type clusters and the fcc slip loop. Energy levels are in units of (kT/ atom); (b) global iso-energy contours for the interaction energy between $(a/2)\langle\bar{1}\,1\,1\rangle$-type clusters and the bcc slip loop. Energy levels are in units of (kT/atom).

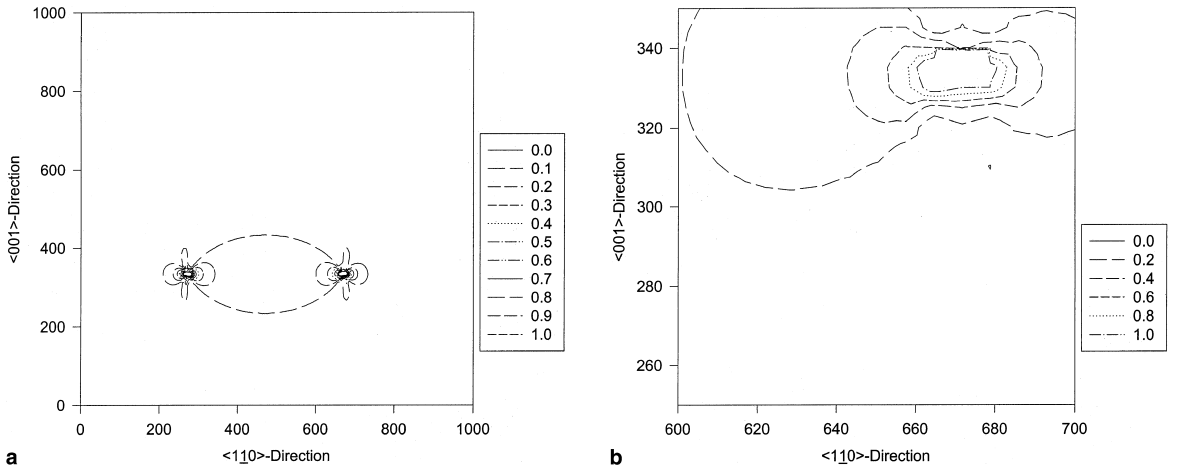

Fig. 13. (a) Global iso-work contours for fcc Cu. On each point on the contour, the dislocation will perform the same amount of work on the cluster to rotate its Burgers vector towards its core; (b) local iso-work contours for the same conditions as in (a). Contour values are in units of 0.1 eV/ atom. The critical surface for Burgers vector rotation is thus the zone enclosed by the contour at a value of unity.

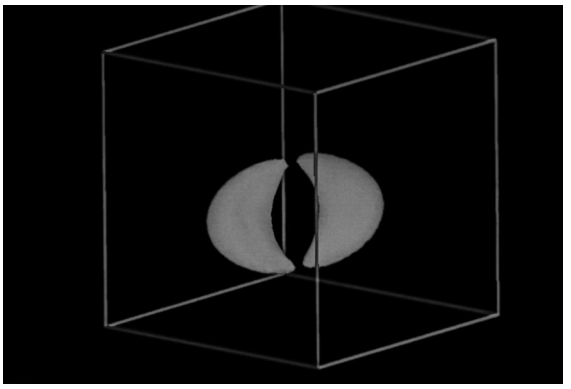

Fig. 14. 3-D iso-energy surface for fcc Cu. The value of the constant energy for this surface is-0.2 kT. It shows the shape of the trapping zones above and below the [1 1 1]-slip plane.

surface splits into two crescent-shape zones, one above and the other below the slip plane. If the slip dislocation attempts to move on its glide plane, the effective elastic potential of trapped clusters will oppose its motion. The magnitude of this opposing force will depend on the character of the loop segment, being greatest at the edge side of the loop.

In fcc metals of low stacking fault energy, small clusters can be in the form of faulted Frank loops. However, if the cluster size is large enough, it is energetically more favorable to unfault and become glissile. In Eq. (14), we compute the energy required to unfault the prismatic cluster dislocation loop. In this energy

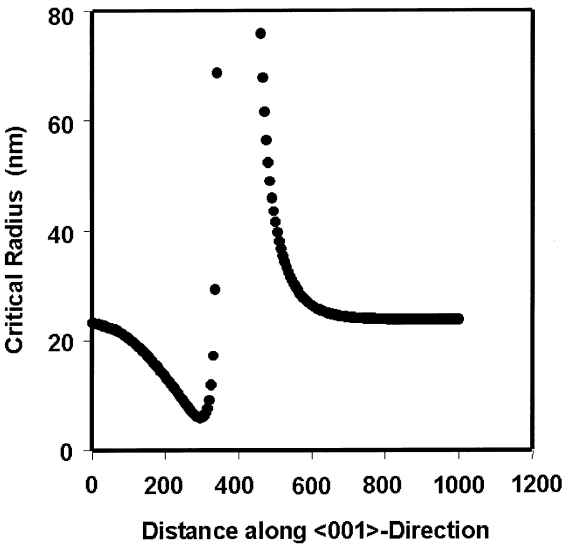

Fig. 15. Dependence of the critical cluster radius for unfaulting on its distance from the dislocation loop core. Clusters with a radius greater than this critical value will unfault, and become glissile.

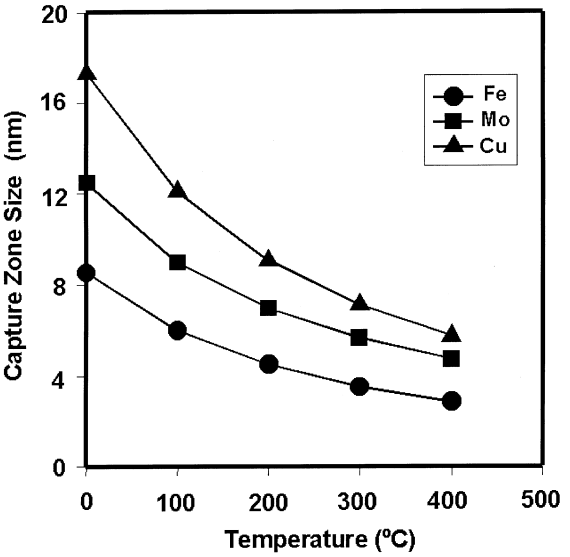

Fig. 16. Temperature dependence of the 'trapping zone size' for small defect clusters in several bcc and fcc materials.

balance, the induced surface tension by the slip loop on the cluster has been taken into account. If clusters are produced very near dislocation cores, it is found that the critical unfaulting radius can be as small as ~6 nm in fcc-Cu. This point is illustrated in Fig. 15, where the critical unfaulting radius is plotted against distance along the ⟨0 0 1⟩-direction in Cu. The stress-free unfaulting radius of ~22 nm is dramatically altered near the core of the slip loop. On the compressive side, the stress field shrinks the critical radius to ~6 nm, while it expands it significantly on the tensile side. Fig. 16 summarizes the temperature dependence of the capture zone size for the three pure metals, Cu, Fe and Mo. As the temperature increases, the elastic modulus decreases, and the thermal energy of the cluster increases. Both factors cooperate to reduce the effective trapping zone at higher temperatures, as can be seen from Fig. 16.

5. Discussion and conclusions

The present study reveals new features of defect cluster interaction with slip dislocations, and is thus complementary to the original work of Trinkaus et al. [11,12]. The interaction between nano-size defect clusters and slip loops is shown to be highly orientation dependent, unlike the situation with point defects represented as centers of dilatation in calculations of dislocation bias factors [19]. The size of the elastic capture zone is primarily determined by the interaction between the edge components of slip loops, and is not very sensitive to

cluster-cluster interaction. Calculated trapping zone sizes are in reasonable agreement with experimental observations.

In bcc crystals, unique interaction energy iso-surfaces for only four independent cluster orientations have been identified. These correspond to clusters with Burgers vectors of the type: $\langle 1\,1\,1\rangle, \langle \bar{1}\,1\,1\rangle$, $\langle \bar{1}\,\bar{1}\,1\rangle$ and $\langle \bar{1}\,1\,\bar{1}\rangle$. Since cluster mobility is constrained by their glide cylinders, the elastic field of slip dislocations can only trap them, if their glide cylinders intersect with energy iso-surfaces whose level is more attractive than cluster thermal energy. Because of this directed motion in bcc crystals, clusters will tend to accumulate just below and above the slip plane, depending on their Burgers vector orientation, and on the character of the adjacent dislocation segment. Maximum cluster trapping is shown to occur near the edge component of a slip loop, while the trapping zone size decreases to zero near purely screw components. It is therefore expected that upon mechanical loading, edge components will be held up by clusters, while screw components will be free to move on the slip plane by glide and out of the plane by cross-slip.

It is also shown that clusters, which are very near dislocation cores (within ~3 nm) can be absorbed into the core by rotation of their Burgers vector as a result of unbalanced torque exerted on them by slip dislocations. If such clusters change the direction of their Burgers vector, they will move toward the dislocation core, and thus will possibly get absorbed. The dynamics of this final step can be ascertained by MD atomistic studies of cluster incorporation into the dislocation core. The distance over which this scenario of cluster incorporation is estimated by the present method to be on the order of ~3 nm for Cu at room temperature. Estimates for the size of the trapping and absorption zones are uncertain, because of the limitations of the model. It is not clear if there are significant effects of elastic anisotropy, and large deformation close to the dislocation core, on the present results, which are obtained by linear isotropic elasticity. More accurate atomistic simulations may shed light on the inherent limitations of our model.

It appears that the initiation of a dislocation channel on the slip plane is associated with the stress required for the dislocation to overcome the collective elastic potential of trapped clusters. This possibility is rather high in bcc crystals, and is a consequence of the high mobility of irradiation defect clusters. It remains to be seen, however, whether the plastic instability is initiated by 'absorption' of small defect clusters, once they rotate their Burgers vector toward the dislocation core, or is a result of the leading dislocation 'sweeping' these small clusters. The answer to this question may require dedicated experiments, as well as dynamical computer simulations. Both MD (e.g., Ref. [20]), and dislocation dynamics (DD) may be required to resolve this question. In either scenario, the type of radiation hardening in bcc metals appears to be of a 'Cottrell' nature, similar to hardening by impurity clouds in alloys. This in contrast to hardening by dislocations cutting through dispersed barriers on the glide plane in the normal Orowan mechanism.

Several features of cluster–dislocation interactions in fcc crystals are differentiated from the conclusions on bcc crystals. Small prismatic defect clusters in fcc crystals are sessile, because of the low stacking fault energy. They immediately dissociate into Schockley partial dislocations, with out-of-plane Burgers vector, rendering them sessile. However, we have shown that an 'induced surface tension' is provided if clusters are nucleated near dislocation cores, or even if moving dislocations interact with them, thus altering the energy balance for their dissociation into partials. In either one of these two possibilities, dissociated, sessile clusters in fcc crystals may be converted to a glissile configuration. If this condition were satisfied, it would potentially lead to the initiation of a plastic instability and the formation of clear channels. These scenarios cannot be asserted without further analysis with molecular (MD) and dislocation (DD) types of dynamic simulations.

It is shown here that the trapping, or 'capture' distance in Cu is on the order of 20 nm at room temperature, while the corresponding absorption zone is ~6 nm. The temperature dependence of both zones in Cu is stronger than in Fe, because their size shrinks by a factor of two at half the melting point. These estimates should be checked by mechanistic experiments, where determination of the trapping zone size is systematically studied for several pure materials as a function of the irradiation temperature. Earlier estimates by Trinkaus et al. [11,12] show that the trapping zone size for a cluster containing only 10 crowdions to be ~90 nm, and that the zone size increases linearly with the number of crowdions in the cluster. If we consider mobile clusters containing hundreds of interstitial atoms, as in the present study, their estimated trapping zone size would be on the order of several 1000 nm. The reader should be aware of the origin of this discrepancy, as it is only related to the microscopic model for cluster motion. Detailed experimental observations may more exactly determine the 3-dimensional structure and extent of cluster accumulation zones around dislocation loop segments, while MD computer simulations are required to ascertain the size dependence of cluster mobility. Recent MD computer simulations by Stoller et al. [21] indicate that for the a cluster of only 19 interstitials in Fe, the activation energy is on the order of 0.1 eV, which is essentially the migration energy of a single interstitial (see also [8,9]).

Acknowledgements

The authors would like to acknowledge discussions with Dr Trinkaus and the useful comments provided by Dr Osetsky. Research is supported by the US Department of Energy, Office of Fusion Energy, Grant #DE-FG03-98ER54500, and the Materials Research Institute (MRI) at Lawrence Livermore National Laboratory, Grant #MI-99-017 with UCLA, and is partially funded by the European Fusion Technology program.

References

[1] B.N. Singh, A.J.E. Foreman, H. Trinkaus, J. Nucl. Mater. 249 (1997) 103.
[2] Y. Dai, PhD thesis (No. 1388), University of Lausanne, Swizerland, 1995.
[3] B.N. Singh, J.H. Evans, A. Horsewell, P. Toft, D.J. Edwards, J. Nucl. Mater. 223 (1995) 95.
[4] B.N. Singh, J.H. Evans, A. Horsewell, P. Toft, G.V. Müller, J. Nucl. Mater. 258 (1998) 865.
[5] Yu.N. Osetsky, M. Victoria, A. Serra, S.I. Golubov, V. Priego, J. Nucl. Mater. 251 (1997) 34.
[6] T. Diaz de la Rubia, M. Guinan, Phys. Rev. Lett. 66 (1991) 2766.
[7] D.J. Bacon, T. Diaz de la Rubia, J. Nucl. Mater. 216 (1994) 275.
[8] Yu.N. Osetsky, A. Serra, V. Priego, Mater. Res. Soc. Symp. Proc. 25 (1998) 59.
[9] Yu.N. Osetsky, D.J. Bacon, A. Serra, B.N. Singh, S.I. Golubov, these Proceedings, p. 65.
[10] W. Sigle, M.L. Jenkins, J.L. Hutchison, Philos. Mag. Lett. 57 (1988) 2766.
[11] H. Trinkaus, B.N. Singh, A.J.E. Foreman, J. Nucl. Mater. 249 (1997) 91.
[12] H. Trinkaus, B.N. Singh, A.J.E. Foreman, J. Nucl. Mater. 251 (1997) 172.
[13] B.N. Singh, J. Evans, unpublished work.
[14] N.M. Ghoniem, ASME J. Eng. Mater. Tech. 121 (1999) 136.
[15] N.M. Ghoniem, L. Sun, Phys. Rev. B 60 (1) (1999) 128.
[16] F. Kröner, Ergeb. Angew. Math. 5 (1958) 1.
[17] R. DeWit, Sol. State Phys. 10 (1960) 249.
[18] F. Kroupa, in: B. Gruber (Ed.), Theory of Crystal Defects, Academia Publishing, Prague, 1966, p. 275.
[19] R. Bullough, J.R. Willis, Philos. Mag. 31 (1975) 855.
[20] A.J.E. Forman, C.A. English, W.J. Phythian, Philos. Mag. A 66 (1992) 655.
[21] R.E. Stoller, G.R. Odette, B.D. Wirth, J. Nucl. Mater. 251 (1997) 49.